PCCP

PAPER

View Article Online
View Journal | View Issue

Cite this: *Phys. Chem. Chem. Phys.*, 2025, **27**, 15435

An all-atom force field for MD simulations on organosulfur and organohalogen active pharmaceutical ingredients developed from experimental sublimation enthalpies and single crystal X-ray diffraction data†

Cátia S. D. Lopes, Manuel E. Minas da Piedade and Carlos E. S. Bernardes *

Received 28th March 2025,
Accepted 29th June 2025

DOI: 10.1039/d5cp01216c

rsc.li/pccp

An all-atom force field for MD simulations on crystalline Active Pharmaceutical Ingredients (API) containing sulfur and halogens was developed and tested. Validation was performed by comparing the MD results with enthalpies of sublimation experimentally determined by Calvet microcalorimetry and reported single crystal X-ray diffraction data. The test set consisted of sulfanilamide, sulfapyridine, chlorzoxazone, clioquinol, and triclosan. The development was incremental. The OPLS-AA model was taken as the starting point. Then dihedral parameters missing in the OPLS-AA database were obtained from PES data computed at the MP2/aug-cc-pVDZ level of theory. Finally, several methods to determine atomic point charges were tested and a procedure based on the ChelpG methodology, with the inclusion of X-sites mimicking the σ-hole in the case of iodine, was found to provide the best overall accuracy in terms of unit cell dimensions and enthalpy of sublimation predictions.

1 Introduction

Molecular dynamics (MD) simulations have become a powerful tool to obtain microscopic insights into many chemical and physical properties of liquids, solutions, and solid materials.[1] In the case of crystalline organic compounds, such as most active pharmaceutical ingredients (API), this theoretical approach has proven valuable to investigate aspects as diverse as solubility,[2–4] crystallization,[5–7] or polymorphism,[8,9] just to name a few.

At the heart of MD simulations is the force field, which describes the intermolecular and intramolecular interactions present in the crystal lattice. Force field models typically rely on atom–atom pair potentials, including terms that model van der Waals (VDW) interactions (*e.g.*, 12-6 Lennard-Jones or Buckingham functions) and atomic point charges (APCs) that account for Coulomb interactions.[10] Over the years, numerous force field parameterizations have been proposed and refined to describe the atom–atom interactions.[10] For simulations involving solid materials a common practice consists in extracting VDW and intramolecular parameterizations from well-established sources (*e.g.* OPLS-AA,[11] AMBER,[12] and W99[13]) and calculating APCs for each molecule using quantum chemistry methods.[14,15] The rationale behind this approach lies in the reasonably good transferability of VDW parameters for a given atom type.[15] APCs are, however, significantly more sensitive to atomic connectivity/molecular environment. Various approaches have been proposed to obtain atomic point charges and describe electrostatic interactions in molecular organic solids, including the ChelpG,[16] RESP,[17] and PIXEL[18] procedures, as well as the use of distributed multipole models.[19]

In previous studies, we have emphasized the importance of validating the development of force fields for MD simulations against both structural and energetic experimental data, namely, unit cell dimensions and standard molar enthalpies of sublimation ($\Delta_{sub}H^0_m$), the latter reflecting the lattice energy of the crystal.[14,20–22] Information on the crystal structures of a vast number of organic compounds is available in the

Centro de Química Estrutural, Institute of Molecular Sciences, Departamento de Química e Bioquímica, Faculdade de Ciências, Universidade de Lisboa, Campo Grande, 1749-016 Lisboa, Portugal. E-mail: cebernardes@ciencias.ulisboa.pt

† Electronic supplementary information (ESI) available: Fig. S1–S10 with the ^{1}H-NMR spectra. Tables S1–S5 with the results of powder X-ray diffraction indexation. Fig. S11–S13 and Tables S6–S11 with the differential scanning calorimetry results. Tables S12–S21 with the Calvet-drop microcalorimetry results. Table S22 with the coefficients of eqn (7). Table S23 with details of the revision of enthalpy of sublimation data from literature. Fig. S14 showing the atoms labeling scheme used in the MD simulations. Tables S24–S28 with the APCs used in the MD simulations. Tables S29–S32 with the comparison between the experimental and MD simulation results. Files with the atomic coordinates of the optimized molecular structures used in the APCs calculations, and files used to prepare the MD simulations using the program DLPGEN (including a file with the force field parametrization). See DOI: https://doi.org/10.1039/d5cp01216c

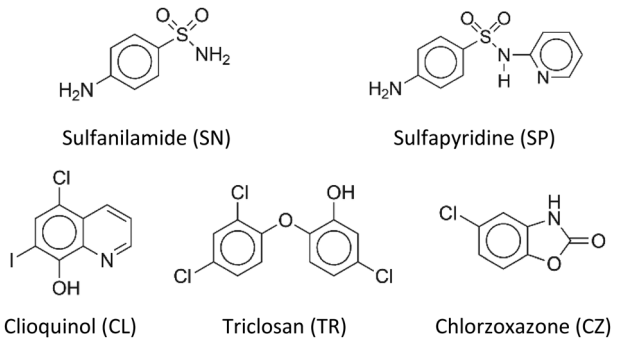

Fig. 1 Molecular structures of the compounds investigated in this work.

Cambridge Structural Database.[23] Enthalpies of sublimation that can be linked to a specific crystal structure are, however, rather scarce.[20,24–27] It is also fairly common that the crystal structures and $\Delta_{sub}H^0_m$ values reported for a specific compound do not refer to the same temperature, an aspect that adds another level of complexity to the benchmarking. The need to overcome these problems has fostered a very recent European initiative, the COST Action CA22107 (**https://bestcsp.eu/about/**), which brings together leading experimental groups focused on the determination of structural and thermodynamic data, and simulation groups engaged in the development of methodologies for the prediction of crystal structures, thermodynamic properties, and spectroscopic properties of molecular organic solids.

In this work, we developed a force field model for MD simulations of organosulfur and organohalogen compounds. The selected test set consisted of five APIs containing S, Cl, and I (Fig. 1), namely sulfanilamide (SN), sulfapyridine (SP), chlorzoxazone (CZ), clioquinol (CL), and triclosan (TR). The force field development was incremental, and the validation was based on reported unit cell dimensions for specific crystal forms of the test set and on corresponding $\Delta_{sub}H^0_m$ values here determined using Calvet-drop sublimation microcalorimetry.

2 Materials and methods

2.1 General

Elemental analyses (EA; C, H, N, S) were performed on a Fisons Instruments EA1108 apparatus. The results correspond to the molar percentage of the mean of two determinations and the uncertainties quoted are twice the average absolute deviation of the determinations.

Reversed-phase high-performance liquid chromatography–electrospray mass spectrometry (HPLC–ESI/MS) was carried out on a Dionex Ultimate 3000 HPLC apparatus, equipped with a HPG3200 binary pump, a WPS300 autosampler, a TCC3000 column oven, and a DAD 3000 detector. This system was coupled in-line to an LCQ Fleet ion trap mass spectrometer including an ESI ion source from Thermo Scientific. The Xcalibur software was used to obtain and process the data. Methanolic solutions were prepared and injected into a Phenomenex Luna C18 column (150 mm × 2 mm, 5 μm) kept at 303 K. The separation was performed with a flow rate of 4.17×10^{-3} cm^3 s^{-1}, using a mobile phase consisting of 0.1% (v/v) formic acid in water (eluent A) and acetonitrile (eluent B), with the following gradient elution program: (i) 120 s isocratic 5% B; (ii) 1080 s linear gradient to 70% B; (iii) 120 s linear gradient to 100% B; (iv) 480 s isocratic 100% B; and (v) 300 s linear gradient to 5% B. Afterwards a re-equilibration time of 600 s for the column was used. The mass spectra were obtained in the ESI (+/−) ion modes from 100 to 700 Da, with an average of 20 to 35 scans. The following optimized parameters were used: ion spray voltage, ±4.5 kV; capillary voltage, +16 V or −18 V; tube lens offset, −70 V or +58 V; sheath gas (N_2) pressure, 80 arbitrary units; auxiliary gas (N_2) pressure, 5 arbitrary units; capillary temperature, 543 K.

Nuclear magnetic resonance (NMR) analyses were performed on a Bruker Ultrashield 400 MHz spectrometer, at 295 ± 2 K. The ^{1}H-NMR were obtained using solutions of the compounds in hexadeuterodimethyl sulfoxide (DMSO-d_6, Sigma-Aldrich, 99.9 atom% D).

Powder X-ray diffraction (PXRD) experiments were carried out at 293 ± 1 K, on a Philips X'Pert PRO apparatus equipped with a PW 3050/60 vertical goniometer and a X'Celerator detector. The X'Pert Data Collector v2.0b software was used for automatic data acquisition. The radiation source was a Cu-K$_\alpha$ tube (λ = 1.5406 Å), operated at 40 kV and 30 mA. The data collection was performed in continuous mode, with a scan step of 20 s and a step size of 0.017° (2θ). The 2θ range covered was 7° to 35°. The samples were placed on a silicon sample holder. The indexation of the powder patterns was done with the CELREF software.[28] The uncertainties of the lattice parameters correspond to standard deviations (u) calculated as previously described.[29]

Differential scanning calorimetry (DSC) experiments were performed on a PerkinElmer DSC 7. The apparatus was controlled by a TAC 7/DX thermal analysis unit and the Pyris V. 7.0 software. The temperatures of fusion (T_{fus}, taken at the onset of the fusion peak) and corresponding specific enthalpies of fusion ($\Delta_{fus}h$/J g^{-1}) were determined at a heating rate of 5 K min^{-1} under a nitrogen (Praxair 5.0) flow of 30 cm^3 min^{-1}. The calibration of the temperature and enthalpy scales of the apparatus was carried out at the same heating rate, and was based on a previously described procedure that relies on the temperatures and enthalpies of fusion of several reference materials.[30] The samples with 1–11 mg mass, were weighed with a precision of ±0.1 μg on a Mettler XP2U ultra-micro balance, and sealed in air inside aluminum crucibles. The temperatures (T_{fus},) and standard molar enthalpies of fusion ($\Delta_{fus}H^0_m$) obtained from the DSC experiments are means of five replicates and the associated errors correspond to expanded uncertainties for 95% confidence level ($2u_c$).

2.2 Materials

Sulfanilamide (SN; TCI, 99.7%) was used as received. EA for $C_6H_8N_2O_2S$: expected C 41.85%, H 4.68%, N 16.27%, S 18.62%; found C 41.98 ± 0.20%, H 4.76 ± 0.02%, N 16.39 ± 0.06%, S 19.08 ± 0.08%. ^{1}H-NMR analysis (400 MHz, DMSO-d_6;

see ESI†): δ/ppm = 7.45 (d, C**H**, 2H, H_4), 6.90 (s, N**H**, 2H, H_6), 6.59 (d, C**H**, 2H, H_3), 5.81 (s, N**H**, 2H, H_1). The powder pattern was indexed as β-SN, monoclinic, space group $P2_1/c$, Z = 4, a = 899.4 ± 0.9 pm, b = 902.3 ± 0.4 pm, c = 1005.2 ± 1.1 pm, β = 111.52 ± 0.10°, and density ρ = 1507.4 ± 5.1 kg m^{-3} (see ESI†). These results are in agreement with the single crystal X-ray diffraction data previously reported for β-SN at 295 K (CSD refcode SULAMD03):[23,31] monoclinic, space group $P2_1/c$, Z = 4, a = 897.5 ± 0.3 pm, b = 900.5 ± 0.3 pm, c = 1003.9 ± 0.4 pm, β = 111.43 ± 0.05°, and density ρ = 1514.5 ± 2.1 kg m^{-3}. The DSC traces (see ESI†) revealed a β to γ phase transition at with a peak maximum at T_{max} = 370.7 ± 1.0 K and $\Delta_{trs}H^0_m$ = 1.3 ± 0.2 kJ mol^{-1}. This thermal event was followed by the fusion of phase γ with T_{fus} = 438.1 ± 0.0 K, T_{max} = 439.7 ± 0.1 K, and $\Delta_{trs}H^0_m$ = 23.5 ± 0.2 kJ mol^{-1}. These results are compatible with previously reported values, obtained at higher heating rates (10 and 20 K min^{-1}) than that employed in this work (5 K min^{-1}): T_{trs} = 407.0 K and $\Delta_{trs}H^0_m$ = 1.63 kJ mol^{-1};[32] T_{trs} = 381.9–401.8 K and $\Delta_{trs}H^0_m$ = 1.6–1.9 kJ mol^{-1};[33] T_{fus} = 435.4 K and $\Delta_{fus}H^0_m$ = 23.28 ± 0.79 kJ mol^{-1};[34] T_{fus} = 434.8–437.8 K and $\Delta_{fus}H^0_m$ = 22.2–23.1 kJ mol^{-1};[33] T_{fus} = 438.8 ± 1.2 K and $\Delta_{fus}H^0_m$ = 22.7 ± 1.9 kJ mol^{-1};[35] T_{fus} = 439.3 K, and $\Delta_{fus}H^0_m$ = 24.02 kJ mol^{-1};[32] T_{fus} = 347.6 K, and $\Delta_{fus}H^0_m$ = 23.4 kJ mol^{-1}.[36]

Sulfapyridine (SP; Acrös Organics, 99.9%), was used as received. EA for $C_{11}H_{11}N_3O_2S$: expected C 53.00%, H 4.45%, N 16.86%, S 12.86%; found C 53.26 ± 0.26%, H 4.58 ± 0.12%, N 16.61 ± 0.12%, S 12.35 ± 0.12%. ^{1}H-NMR analysis (400 MHz, DMSO-d_6; see ESI†): δ/ppm = 10.92 (s, N**H**, 1H, H_6), 8.09 (d, C**H**, 1H, H_{11}), 7.64 (t, C**H**, 1H, H_{10}), 7.51 (d, C**H**, 2H, H_4), 7.06 (d, C**H**, 1H, H_8), 6.89 (t, C**H**, 1H, H_9), 6.54 (d, C**H**, 2H, H_3), 5.93 (s, N**H**$_2$, 2H, H_1). The powder pattern was indexed as SP form III, monoclinic, space group $C2/c$, Z = 8, a = 1271.5 ± 3.8 pm, b = 1166.9 ± 2.7 pm, c = 1537.3 ± 5.7 pm, β = 93.70 ± 1.00°, density ρ = 1454.9 ± 15.7 kg m^{-3} (see ESI†). These results are consistent with the single crystal X-ray diffraction data previously reported for SP form III at 298 K (CSD refcode BEWKUJ04):[23,37] monoclinic, space group $C2/c$, Z = 8, a = 1280.7 ± 0.3 pm, b = 1171.1 ± 0.3 pm, c = 1537.9 ± 0.2 pm, β = 94.07 ± 0.02°, density ρ = 1439.4 ± 1.1 kg m^{-3}. The onset and maximum temperatures of the fusion peak were T_{fus} = 463.4 ± 0.2 K and T_{max} = 466.0 ± 0.1 K, respectively, and the molar enthalpy of fusion was $\Delta_{fus}H^0_m$ = 38.4 ± 0.1 kJ mol^{-1}. These results are in good agreement with the recently published T_{fus} = 464.2 ± 0.1 K and $\Delta_{fus}H^0_m$ = 38.7 ± 0. 4 kJ mol^{-1},[38] and T_{fus} = 462.0 ± 2.0 K and $\Delta_{fus}H^0_m$ = 38.7 ± 1.2 kJ mol^{-1},[38] obtained by conventional DSC and fast scanning calorimetry, respectively. They are also, in most cases, compatible with other literature values determined at a higher heating rate (10 K min^{-1}) than that employed in this work (5 K min^{-1}): T_{fus} = 462.7 K and $\Delta_{fus}H^0_m$ = 40.47 ± 0.14 kJ mol^{-1};[34] T_{fus} = 464.77 K and $\Delta_{fus}H^0_m$ = 33.31 kJ mol^{-1};[39] T_{fus} = 463.95 K and $\Delta_{fus}H^0_m$ = 44.06 kJ mol^{-1};[40] and T_{fus} = 464.7 K and $\Delta_{fus}H^0_m$ = 38.8 kJ mol^{-1}.[36] It should also be noted that, in contrast with the present work, all previously reported T_{fus} and $\Delta_{fus}H^0_m$ values for sulfapyridine refer to samples that were not characterized in terms of polymorphism.

Chlorzoxazone (CZ; Alfa Aesar, 98.0%) was purified by sublimation at 1.33 Pa and 343 K. EA $C_7H_4ClNO_2$: expected C 49.58%, H 2.38%, N 8.26%; found C 49.16 ± 0.06%, H 2.16 ± 0.04%, N 8.10 ± 0.02%. The level of impurities in the sublimed sample was below the detection limit of the HPLC-ESI/MS method, suggesting a purity >99.9%. ^{1}H-NMR analysis (400 MHz, DMSO-d_6; see ESI†): δ/ppm = 11.86 (s, N**H**, 1H, H_4), 7.31 (ds, C**H**, 1H, H_2), 7.16 (d, C**H**, 1H, H_7), 7.12 (dd, C**H**, 1H, H_8). The powder pattern was indexed as triclinic, space group $P\bar{1}$, Z = 2, a = 381.7 ± 0.4 pm, b = 902.1 ± 0.8 pm, c = 1004.8 ± 0.8 pm, α = 93.38 ± 0.08°, β = 95.50 ± 0.08°, γ = 98.32 ± 0.09°, density ρ = 1657.2 ± 5.4 kg m^{-3} (see ESI†). These results agree with previously reported single crystal X-ray diffraction data at 295 K (CSD refcode NEWKOP):[23,41] triclinic, space group $P\bar{1}$, Z = 2, a = 381.5 ± 0.1 pm, b = 903.8 ± 0.1 pm, c = 1006.3 ± 0.1 pm, α = 93.35 ± 0.01°, β = 95.52 ± 0.01°, γ = 98.41 ± 0.01°, density ρ = 1652.8 ± 1.0 kg m^{-3}. The onset and maximum temperatures of the fusion peak were T_{fus} = 463.6 ± 0.2 K and T_{max} = 465.3 ± 0.2 K, respectively, and the molar enthalpy of fusion was $\Delta_{fus}H^0_m$ = 25.8 ± 0.2 kJ mol^{-1} (see ESI†). These results are consistent with T_{fus} = 464.2 K and $\Delta_{fus}H^0_m$ = 25.62 kJ mol^{-1}, previously determined at a heating rate of 10 K min^{-1}.[42]

Clioquinol (CL; Maybridge, 95.0%) was purified by sublimation at 1.33 Pa and 368 K. EA for C_9H_5ClNO: expected C 35.38%, H 1.65%, N 4.58%; found C 35.84 ± 0.22%, H < 2%, N 4.56 ± 0.02%. The level of impurities in the sublimed sample was below the detection limit of the HPLC-ESI/MS method, suggesting a purity >99.9%. ^{1}H-NMR analysis (400 MHz, DMSO-d_6; see ESI†): δ/ppm = 8.96 (d, C**H**, 1H, H_5), 8.48 (d, C**H**, 1H, H_7), 7.98 (s, C**H**, 1H, H_{10}), 7.76 (m, C**H**, 1H, H_6). The powder pattern recorded at 293 ± 2 K, was indexed as monoclinic, space group $P2/c$, Z = 4, a = 1455.4 ± 2.2 pm, b = 412.7 ± 0.8 pm, c = 1660.5 ± 2.4 pm, β = 111.63 ± 0.14°, density ρ = 2188.5 ± 13.5 kg m^{-3} (see ESI†). These results agree with the published single crystal X-ray diffraction data at 296 K (CSD refcode CIQUOL02):[23,43] monoclinic, space group $P2/c$, Z = 4, a = 1446.28 ± 0.10 pm, b = 409.86 ± 0.03 pm, c = 1653.36 ± 0.11 pm, β = 111.379 ± 0.002°, density ρ = 2223.1 ± 0.4 kg m^{-3}. The DSC curves obtained for CL revealed a reversible phase transition characterized on heating mode by onset temperature T_{trs} = 381.2 ± 0.6 K and enthalpy $\Delta_{trs}H^0_m$ = 0.5 ± 0.2 kJ mol^{-1}, and on cooling mode by onset temperature T_{trs} = 367.9 ± 1.6 K and enthalpy $\Delta_{trs}H^0_m$ = −0.3 ± 0.7 kJ mol^{-1} (Fig. S13 and Tables S9, S10 in the ESI†). To the best of our knowledge this phase transition had not been previously reported. Nevertheless, because the sublimation experiments on clioquinol were performed below this temperature the obtained enthalpy of sublimation can be safely assigned to the monoclinic form mentioned above (CSD refcode CIQUOL02). After the solid–solid phase transition, the fusion of the compound was recorded with the onset and maximum temperatures at T_{fus} = 453.0 ± 1.0 K, T_{max} = 454.9 ± 0.6 K, and molar enthalpy of fusion $\Delta_{fus}H^0_m$ = 23.6 ± 2.2 kJ mol^{-1}. The later values should, however, be considered with caution due to the decomposition of the material on melting. The T_{fus} here obtained is lower than that previously reported by Padmanabhan *et al.*, T_{fus} = 458.15 K,[44] which corresponds to a heating rate of 10 K min^{-1}. Because in the later study, the crystal form used was not identified and no

phase transition was reported, the difference in the fusion temperatures may suggest that different polymorphs were investigated here and by Padmanabhan *et al.*[44]

Triclosan (TR; Alfa Aesar, 99.7%) was sublimed at 1.33 Pa and 328 K prior to use. EA for $C_{12}H_7Cl_3O_2$: expected C 49.78%, H 2.44%; found C 49.40 ± 0.08%, H 2.23 ± 0.04%. The level of impurities in the sublimed sample was below the detection limit of the HPLC-ESI/MS method, suggesting a purity > 99.9%. ^{1}H-NMR analysis (400 MHz, DMSO-d_6; see ESI†): δ/ppm = 10.33 (s, O**H**, 1H, H_{11}), 7.69 (s, C**H**, 1H, H_{13}), 7.31 (d, C**H**, 1H, H_2), 7.02 (d, C**H**, 1H, H_6), 7.01 (s, C**H**, 1H, H_9), 6.88 (d, C**H**, 1H, H_7), 6.73 (d, C**H**, 1H, H_3). The powder pattern recorded at 293 ± 2 K, was indexed as trigonal, space group $P3_1$, Z = 3, a = 1264.4 ± 0.9 pm, b = 1264.4 ± 0.4 pm, c = 672.1 ± 1.1 pm, density ρ = 1550.1 ± 6.4 kg m^{-3} (see ESI†). These results are consistent with published data from single crystal X-ray diffraction experiments carried out at 293 K (CSD refcode QUBQIO01):[45] trigonal, space group $P3_1$, Z = 3, a = 1264.1 ± 0.0 pm, b = 1264.1 ± 0.0 pm, c = 671.6 ± 0.0 pm, crystal density ρ = 1551.9 ± 0.1 kg m^{-3}. The onset and maximum temperatures of the fusion peak were T_{fus} = 328.7 ± 0.5 K and T_{max} = 332.0 ± 0.3 K, respectively, and the molar enthalpy of fusion was $\Delta_{fus}H^0_m$ = 26.0 ± 0.4 kJ mol^{-1}. The origin of the discrepancy between the DSC results obtained here and the previously reported,[46] T_{fus} = 331.05 K and $\Delta_{fus}H^0_m$ = 17.75 kJ mol^{-1}, was impossible to assess since in the latter case, the crystal form used was not identified and no details regarding the experiments from which T_{fus} and $\Delta_{fus}H^0_m$ were obtained, or uncertainties of the results, were given by the authors.

2.3 Calvet-drop microcalorimetry

Enthalpies of sublimation or vaporization were determined using the Calvet-drop microcalorimetry apparatus and experimental procedure previously described.[47,48] In a typical experiment, samples with a mass of 1–6 mg were placed inside glass capillaries and weighted with a precision of ±0.1 μg on a Mettler UMT2 ultramicro balance. The capillary was placed inside the drop furnace and left to equilibrate at T_i ∼ 298.15 K for ∼1800 s. After a suitable baseline was acquired, the capillary was dropped into the calorimetric cell whose temperature was set to T_f = 419.1 K for SN, T_f = 423.9 K for SP, T_f = 419.3 K for CZ, T_f = 369.7 K for CL, and T_f = 351.4 K for TR. The curve corresponding to the heating of the sample and capillary from T_i to T_f (which in the case of triclosan also included melting at 328.7 ± 0.5 K) was recorded, and once the signal returned to the baseline, the sample and reference cells were simultaneously evacuated to 0.13 Pa. This started the sublimation/vaporization process, which was monitored until the signal returned to the baseline. The area, A, of the corresponding curve is related to the specific sublimation/vaporization enthalpy, $\Delta_{sub/vap}h$, by:

$$\Delta_{sub/vap}h = \frac{\varepsilon(A - A_b)}{m} \quad (1)$$

where m corresponds to the mass of sample; A_b is the contribution to the overall area due to pumping the air from the calorimetric cell, which was obtained from a series of independent experiments where the calorimetric cells containing only air were evacuated; and ε is the energy equivalent of the calorimeter, determined by electrical calibration, using the following equation:

$$\varepsilon = \frac{\sum_i V_i I_i \Delta t_i}{A_c} \quad (2)$$

Here V_i and I_i represent the potential difference and current intensity, respectively, across a 200 Ω electric resistance placed inside the sample cell; Δt_i ∼ 1 s is the time step between two consecutive data acquisitions; and A_c is the area of the calibration curve. Calibrations were carried out at each temperature selected to study a given system.

The calculation of standard molar enthalpies of sublimation, $\Delta_{sub}H^0_m$, at 298.15 K from the obtained $\Delta_{sub/vap}h$ values relied on the equation:

$$\Delta_{sub}H^0_m(298.15) = M \cdot \Delta_{sub/vap}h(T_f) + \Delta^{g,298.15K}_{g,T_f}H^0_m - \Delta^{cr,298.15K}_{cr/l,T_f}H^0_m \quad (3)$$

where M is the molar mass of the compound, and $\Delta^{cr,298.15K}_{cr/l,T_f}H^0_m$ and $\Delta^{g,298.15K}_{g,T_f}H^0_m$ represent the enthalpy corrections needed to bring the crystal/liquid and gas phases at T_f to solid and gas phases at 298.15 K, respectively. The first term was obtained from the area, A_h, of the curve associated with heating the sample from T_i to T_f (which, as mentioned above also reflects melting in the case of triclosan) using the equation:

$$\Delta^{g,298.15K}_{g,T_f}H^0_m = \frac{M}{m}\left[\varepsilon \cdot A_h - m_{cap} \cdot c_{p,glass} \cdot (T_f - T_i)\right] \quad (4)$$

Here m_{cap} and $c_{p,glass}$ are the mass and specific heat capacity of the glass capillary in the temperature range T_i to T_f, respectively. The average value of $c_{p,glass}$ in the different temperature ranges used in the experiments was obtained from:

$$c_{p,glass} = \frac{\varepsilon \cdot A_{glass}}{m_{cap} \cdot (T_f - T_i)} \quad (5)$$

in a series of experiments where empty glass capillaries were placed inside the drop furnace at T_i ∼ 298.15 K and dropped into the measuring cell at T_f, leading to a heating curve of area A_{glass}.

The enthalpy correction for the gas phase was evaluated from:

$$\Delta^{298.15K}_{T_f}H^0_m(g) = \int_{T_f}^{298.15} C^0_{p,m}(g)\mathrm{d}T \quad (6)$$

where $C^0_{p,m}(g)$ represents the standard molar heat capacity. The $C^0_{p,m}(g)$ *vs.* T functions for each system in the range 200 to 400 K, were obtained from a least squares fit of the equation:

$$C^0_{p,m}(g)/(\mathrm{J\ K^{-1}\ mol^{-1}}) = a(T/\mathrm{K})^2 + b(T/\mathrm{K}) + c \quad (7)$$

to the data computed by the statistical mechanics and quantum chemistry procedures, described in the next section. The values of the a, b, and c coefficients are given as ESI† (Table S22).

For all compounds, visual inspection of the calorimetric cell and the capillary after the sublimation experiments showed no evidence of residues indicating sample decomposition. Furthermore, ^{1}H-NMR analysis of materials sublimed at the

same temperatures used in the Calvet-drop microcalorimetry runs demonstrated that no decomposition occurred during the solid → gas transition (see ESI†).

2.4 Quantum chemistry modelling

For sulfanilamide, sulfapyridine, chlorzoxazone, and triclosan, the $C^0_{p,m}(g)$ data needed to correct the calorimetrically measured $\Delta_{sub}H^0_m$ values from the temperature of the experiments to 298.15 K (eqn (6)), were calculated by statistical thermodynamics,[49] using harmonic vibration frequencies computed at the B3LYP/aug-cc-pVDZ level of theory[50–53] and scaled by 0.970.[54] In the case of CL, iodine was modeled with the 6-311G(d,p) basis set (the corresponding aug-cc-pVDZ basis set is not available)[55,56] and the aug-cc-pVDZ basis set was used for all other elements. The CL vibration frequencies were also scaled by 0.970. The calculations were performed using Gaussian-09.[57]

The atomic point charges needed for the MD simulations were computed by the ChelpG[16] and RESP[58] methodologies using Multiwfn 3.8.[59] The wavefunctions were obtained with ORCA 5.0.4,[60] using the B3LYP-D3[52,61,62] model with the def2-TZVP[63] basis set, the def2/J[64] auxiliary basis set, and the RIJCOSX approximation.[65] These calculations were preceded by a molecular structure optimization with the composite model B97-3c.[66] The above models and basis sets were selected to allow the same type of approach for all compounds, independently of the elements and number of atoms (*e.g.*, some of the calculations included clusters of molecules with more than 100 atoms). Files with the atomic coordinates obtained after structure optimization are provided as ESI.†

The potential energy barriers associated with dihedral angle rotations were obtained from potential energy scans (PES) carried out at the MP2/aug-cc-pVDZ[51,53,67,68] level of theory using Orca 5.0.4.[60]

2.5 Molecular dynamics simulations

Unless otherwise stated, MD simulations were performed with LAMMPS (version 2, Aug 2023)[69] and the input files were prepared with DLPGEN 3.0.[70] The simulation boxes for the crystal phases were set up using single crystal X-ray diffraction data retrieved from the Cambridge Structural Database (CSD refcodes: SULAMD03 for sulfanilamide, BEWKUJ04 for sulfapyridine, NEWKOP for chlorzoxazone, CIQUOL02 for clioquinol, and QUBQIO01 for Triclosan).[23] A cutoff of 1.5 nm was considered in all simulations and several unit cells were stacked along the three-coordinate axes to obtain large enough boxes to accommodate this limit (4–5 nm side). The particle–particle particle–mesh Ewald method was used to compute the electrostatic interactions beyond the cutoff distance.[71] The simulations were run at 298.15 K and 1 bar, employing a Nosé–Hoover thermostat (2 ps time constant) and anisotropic barostat (20 ps time constant), respectively ($N\sigma T$ ensemble). The simulation involved an initial equilibration stage, where the crystals were heated from 10 K to 298.15 K during 1 ns, followed by a 2 ns production stage, at 298.15 K, to obtain the average standard molar configurational internal energy, $U^0_{conf,m}(cr)$, and unit cell parameters. A 2 fs timestep was used for all simulations.

Standard molar enthalpies of sublimation, $\Delta_{sub}H^0_m$, were calculated from:

$$\Delta_{sub}H^0_m = U^0_{conf,m}(g) - U^0_{conf,m}(cr) + RT \quad (8)$$

where $U^0_{conf,m}(g)$ and $U^0_{conf,m}(cr)$ represent the standard molar configurational internal energies in the gas and solid phases, respectively, R = 8.3144626 J K^{-1} mol^{-1} (ref. 72) is the gas constant, and T = 298.15 K. To obtain $U^0_{conf,m}(g)$ 20 independent MD simulation runs of 20 ns duration, were performed under the following conditions: (i) cubic simulation box of 100 nm side, containing a single molecule; (ii) Coulomb and van der Waals (VDW) cutoffs of 20 nm; and (iii) an *NVT* ensemble using a Nosé–Hoover thermostat with a time constant of 1 ps. The average $U^0_{conf,m}(g)$ value resulting from these runs was used in eqn (8).

The configurational internal energies in the solid and gaseous phases were obtained from:

$$\begin{aligned} U_{cfg} &= \sum^{bonds} \frac{k_r}{2}(r-r_0)^2 + \sum^{angles} \frac{k_\theta}{2}(\theta-\theta_0)^2 \\ &+ \sum^{dihedrals} \sum_{n=1}^{4} \frac{V_n}{2}\left[1+(-1)^{(n-1)}\cos(n\varphi)\right] \\ &+ \sum_i \sum_{j>i} \frac{q_i q_j}{4\pi\varepsilon_0 r_{ij}} + 4\varepsilon_{ij}\left[\left(\frac{\sigma_{ij}}{r_{ij}}\right)^{12} - \left(\frac{\sigma_{ij}}{r_{ij}}\right)^{6}\right] \end{aligned} \quad (9)$$

where r and θ are the distances and angles of the bonds and angles in the molecule; r_0 and θ_0 are the equilibrium bond distances and angles in the molecule, respectively; k_r and k_θ, are the force constants of the harmonic oscillators associated with bonds and angles vibrations; V_n are the coefficients of a Fourier series that models the internal rotation of the dihedral angles, φ, in the molecule; ε_0 is the vacuum permittivity; q_i and q_j correspond to atomic point charges (APCs); and ε_{ij} and σ_{ij} are the parameters of the 12-6 Lennard-Jones (LJ) potential.

The force field implementation started from the OPLS-AA scheme,[11] which already includes widely tested parametrizations for a variety of functional groups (particularly, van der Waals terms). This strategy[73] facilitates the extension of force fields to study new types of molecules and complex phenomena (*e.g.* solubility and crystallization) in a straightforward and consistent way.

At the beginning of this work, it was found that several dihedral parameters in the molecules studied were missing in the OPLS-AA database. These were, therefore, obtained by fitting the dihedral term in eqn (9) to PES data computed at the MP2/aug-cc-pVDZ level of theory. The procedure used was previously described[74] and further details are given as ESI.†

To improve the agreement between the computed and experimental enthalpies of sublimation and unit cell parameters, an assessment of MD results based on the original OPLS-AA APC data and on APC values obtained here from DFT calculations was made. The following approaches were used:

• MODEL A. Original OPLS-AA force field charges, q_{opls}.

• MODELS B^C and B^R. APCs computed for an isolated molecule in the gas phase using the ChelpG, q_{gas}^{ChelpG}, and RESP, q_{gas}^{RESP}, methodologies, respectively. In this case, a full geometry optimization of the molecule was run before the APC calculations.

• MODELS C^C and C^R. APCs computed by the ChelpG, q_{cryst}^{ChelpG}, and RESP, q_{cryst}^{RESP}, methodologies, for small clusters of molecules retrieved from the single crystal X-ray diffraction structures. The aggregates were defined by considering a central molecule and all neighbor molecules connected to it by hydrogen or halogen bonds.[14,20] To maintain the relative orientation of the molecules as in the crystal structure, only the position of hydrogens was optimized before APC calculations. The APCs used in the simulations were those obtained for the central molecule.

• MODEL D^C and D^R. APCs, q_{part}^x, computed by using:

$$q_{part}^x = 0.5q_{gas}^x + 0.5q_{cryst}^x \quad (10)$$

where x denotes the ChelpG or RESP charges obtained through models B and C.

Model C is rooted in the previous observation from our group, that using APCs calculated for small clusters of molecules reflecting molecular packing, seems to lead to a better description of the electrostatic interactions in the crystal lattice.[11,16] Model D was inspired by the recently proposed restrained electrostatic potential approach (RESP2).[75] In this case APCs were computed by considering weighed contributions from molecules isolated in the gas phase and solvated. This idea was extended here to crystals based on eqn (10) where q_{gas} refers to an APC obtained for an isolated molecule in the gas phase and q_{cryst} to a central molecule in a cluster mimicking the molecular organization of the crystal lattice. Calculations using ChelpG (MODEL D^C) and RESP (MODEL D^R) procedures were used in conjunction with eqn (10).

In the case of CL, CZ, and TR, halogen bonds are present in the crystal structure. To account for this type of interaction Jorgensen and Schyman[76] proposed the inclusion in the model of "X-sites" located at the σ-hole of the halogen atom (a massless particle located at 180° relative to the C–Cl or C–I bond, with no LJ parameters and charges of 0.075e and 0.110e in the case of chlorine and iodine, respectively), to explicitly describe the formation of halogen bonds. In the present work, two variations of the force field with and without X-sites were considered for CL, CZ, and TR. The implementation closely followed the procedures described by Jorgensen and Schyman.[76] For models B, C, and D, where APCs differed from the OPLS-AA values, charge neutrality was achieved by subtracting the charge of the X-site from that of the corresponding halogen element.

Due to the impossibility of using massless particles in LAMMPS, the simulations of halogenated compounds were made with DL_POLY 4.10.[77] The clioquinol and triclosan molecules were considered flexible, except for the fragments C–Cl–X and C–I–X which were modeled as rigid units. In the case of CZ this approach led to unstable simulations. Since CZ is relatively small and exhibits little flexibility, a fully rigid model was considered in this case.

Full details of the force field parametrization are given as ESI.†

3 Results and discussion

3.1 Standard molar enthalpies of sublimation

The standard molar enthalpies of sublimation at 298.15 K, $\Delta_{sub}H_m^0$ (298.15 K), obtained in this work from Calvet-drop microcalorimetry experiments, are given in Table 1. Also included in the Table 1 are the enthalpies of sublimation or vaporization, $\Delta_{sub/vap}H_m^0(T_f)$, directly measured at the temperature, T_f, of the calorimetric experiments and the correction terms, $\Delta_{g,T_f}^{g,298.15K}H_m^0$ and $\Delta_{cr/l,T_f}^{cr,298.15K}H_m^0$, necessary to convert $\Delta_{sub/vap}H_m^0(T_f)$ to $\Delta_{sub}H_m^0$ (298.15 K).

It is worth noting that attempts to determine $\Delta_{sub}H_m^0$ of sulfonamide compounds other than sulfanilamide and sulfapyridine failed, due to either low vapor pressure (sulfadiazine and sulfamethizole) or decomposition during sublimation (sulfalene and sulfacetamide).

As mentioned in the Materials and methods section, in the case of SN, the experimental sublimation temperature (T_f = 419.10 K) was higher than the temperature at which the β → γ solid–solid phase transition occurs (T_{trs} = 370.7 K). Therefore, the obtained enthalpy value corresponds to the sublimation of

Table 1 Standard (p^0 = 1 bar) molar enthalpy of sublimation and/or vaporization, $\Delta_{sub/vap}H_m^0$, of the compounds studied in this work at the corresponding experiment temperatures, T_f, and after correction to 298.15 K, using eqn (3). For comparison, recomputed values based on available data in the literature are included[a]

Compound	$T_f \pm u$/K	$\Delta_{sub/vap}H_m^0(T_f) \pm U$/kJ mol^{-1}	$-\Delta_{cr/l,T_f}^{cr,298.15K}H_m^0 \pm u$/kJ mol^{-1}	$-\Delta_{g,T_f}^{g,298.15K}H_m^0 \pm u$/kJ mol^{-1}	$\Delta_{sub}H_m^0$ (298.15 K) ± U/kJ mol^{-1} This work	Lit.
β-SN			29.15 ± 0.54[c]	25.68 ± 0.51	130.8 ± 1.2	
γ-SN	419.10 ± 0.01	127.30 ± 1.00[b]			129.5 ± 1.3	
SP	423.94 ± 0.02	147.47 ± 1.28	39.65 ± 0.76	38.39 ± 0.77	148.7 ± 1.7	167.2 ± 4.8[c]
CZ	419.28 ± 0.00	107.07 ± 0.39	21.43 ± 0.49	20.48 ± 0.41	108.0 ± 0.7	
CL	369.72 ± 0.01	110.47 ± 0.99	18.29 ± 0.40	14.04 ± 0.28	114.7 ± 1.1	115.6 ± 1.0[d]
TR	351.44 ± 0.00	89.36 ± 1.02[e]	43.96 ± 0.63	14.20 ± 0.28	119.1 ± 1.2	

[a] Details of the uncertainty calculations are provided as ESI. [b] Uncertainty assuming an arbitrary error of 2% in the computed value. [c] Ref. 38 and Table S23 (ESI). [d] Ref. 78 and Table S23 (ESI). [e] Enthalpy of vaporization of TR at 351.44 K.

form γ at 419.10 K, $\Delta_{sub}H^{o}_{m}$(cr γ, 419.10 K). The enthalpies of sublimation of forms β and γ at 298.15 K, could be determined as $\Delta_{sub}H^{0}_{m}$(cr β, 298.15 K) = 130.8 ± 1.2 kJ mol^{-1} and $\Delta_{sub}H^{0}_{m}$(cr γ, 298.15 K) = 129.5 ± 1.3 kJ mol^{-1} from:

$$\Delta_{sub}H^{0}_{m}(\text{cr }\beta, 298.15\text{ K}) = \Delta_{sub}H^{0}_{m}(\text{cr }\gamma, 419.10\text{ K}) + \Delta^{g,298.15K}_{g,419.10K}H^{0}_{m} - \Delta^{cr\,\beta,298.15K}_{cr\,\gamma,419.10K}H^{0}_{m} \quad (11)$$

$$\Delta_{sub}H^{0}_{m}(\text{cr }\gamma, 298.15\text{ K}) = \Delta_{sub}H^{0}_{m}(\text{cr }\beta, 298.15\text{ K}) + \Delta_{trs}H^{0}_{m}(\beta \rightarrow \gamma) \quad (12)$$

using the $\Delta_{sub}H^{0}_{m}$(cr γ, 419.10 K), $\Delta^{g,298.15K}_{g,419.10K}H^{0}_{m}$, and $\Delta^{cr\,\beta,298.15K}_{cr\,\gamma,419.10K}H^{0}_{m}$ values in Table 1 and $\Delta_{trs}H^{0}_{m}(\beta \rightarrow \gamma)$ = 1.3 ± 0.2 kJ mol^{-1} obtained by DSC at 370.7 ± 1.0 K. The procedure used in the calculation of $\Delta_{sub}H^{0}_{m}$ (298.15 K) for all other molecules is described in the Materials and Methods section (Section 2.3).

To the best of our knowledge, enthalpies of sublimation have only been reported for SP[38] and CL.[78] For consistency in the comparison, all literature results were corrected to 298.15 K using the auxiliary data selected in this work and eqn (3) (see ESI†). The obtained values are listed in Table 1. In the case of CL, there is an excellent agreement between the calorimetric result here obtained, $\Delta_{sub}H^{0}_{m}$ = 114.7 ± 1.1 kJ mol^{-1}, and that reported by Monte and Ribeiro da Silva ($\Delta_{sub}H^{0}_{m}$ = 115.6 ± 1.0 kJ mol^{-1}),[78] from Knudsen effusion measurements on a sample with unspecified phase purity. This is not, however, the case for SP, where a discrepancy of 18.5 kJ mol^{-1} is noted between the results from the present work and those obtained by Nagrimanov *et al.*[38] from vapor pressure measurements by fast scanning calorimetry. The origin of this large discrepancy was impossible to assess, given the nature of the experiments performed by Nagrimanov *et al.*[38] which require melting the compound prior to the sublimation experiments.

3.2 MD simulations

The performance of the different force-field approaches considered here was benchmarked against experimental enthalpies of sublimation and unit cell dimensions of the test set. The results are summarized in Fig. 2 and further details are given as ESI† (Tables S29–S32). Fig. 2 refers to all molecules and models, except that based on the Jorgensen and Schyman[76] approach (''X-sites'' located at the σ-hole of the halogen atom). The latter is specific for halogenated compounds and the corresponding results were, therefore, separately analyzed (Fig. 3).

In terms of structural predictions, Fig. 2a shows that the largest deviations of unit cell parameters (*e.g.* deviations larger than 10% in the case of the *b* and β cell parameters of the SN polymorphs, Table S29, ESI†) are found for the original OPLS-AA parametrization (model A). This is, however, in line with previous observations.[14,20] The best performance was achieved when ChelpG charges were employed (the range of values within the percentile 25–75% is the smallest), particularly when the calculations relied on gas phase (model B^{C}) or averaged APCs (model D^{C}). This is particularly evident in the case of the two polymorphs of SN, for which all tested models (except the original OPLS-AA) reproduced the experimental data with deviations lower than 3.3% (Table S29, ESI†).

The analysis of the difference between the computed enthalpies of sublimation and the corresponding experimental values ($\Delta\Delta_{sub}H$, Fig. 2b), revealed a poorer performance of all models for capturing the lattice energetics compared to volumetric properties. Indeed, while most of the deviations in unit cell dimensions are smaller than *ca.* 4% (Fig. 2a), $\Delta\Delta_{sub}H$ deviations larger than *ca.* 8 kJ mol^{-1} (>7%) were observed, a value significantly larger than the aimed chemical accuracy of 1 kcal ≡ 4.184 kJ mol^{-1}.[79] Nevertheless, the best performance (smaller box amplitude and $\Delta\Delta_{sub}H$ median closer to zero) corresponds to models C^{C}, C^{R}, and D^{C}. This showcases the importance of validating force-field models using both structural and energetic data.

It is interesting to note that of all molecules included in this work, SP is the only one that packs in zwitterionic form. It is also the molecule with the larger deviations between predicted and experimental enthalpy of sublimation values (outliers in Fig. 2b). It can, therefore, be speculated that the VDW

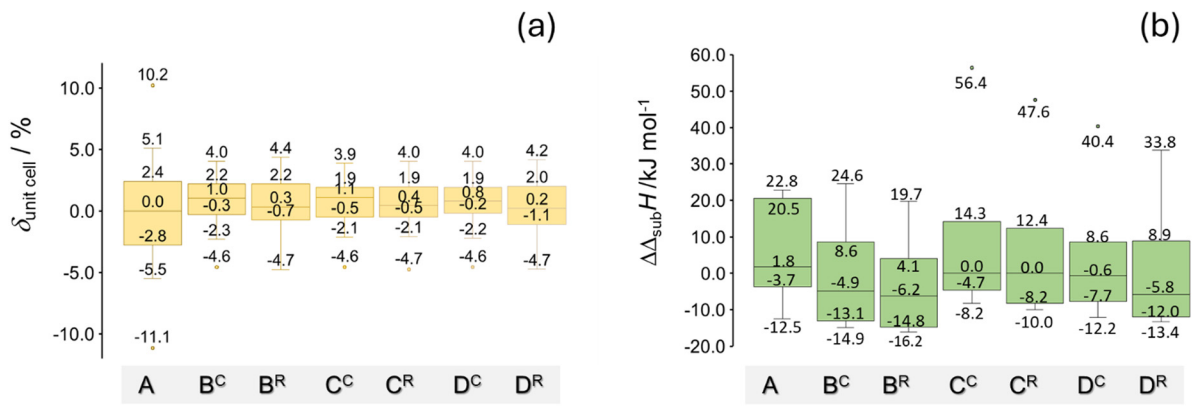

Fig. 2 Evaluation of the performance of the various force field models used in this work through boxplots with whiskers. The boxes represent the interquartile range (IQR), with the central line indicating the median of the values. The upper and lower edges correspond to the 75th and 25th percentiles, respectively. The whiskers extend to the smallest and largest values within 1.5 times the IQR from the quartiles, while individual points beyond this range are considered outliers. (a) Deviation ($\delta_{unit\ cell}$, in percentage) between computed and experimental unit cell parameters; (b) difference between computed and experimental enthalpy of sublimation values ($\Delta\Delta_{sub}H$).

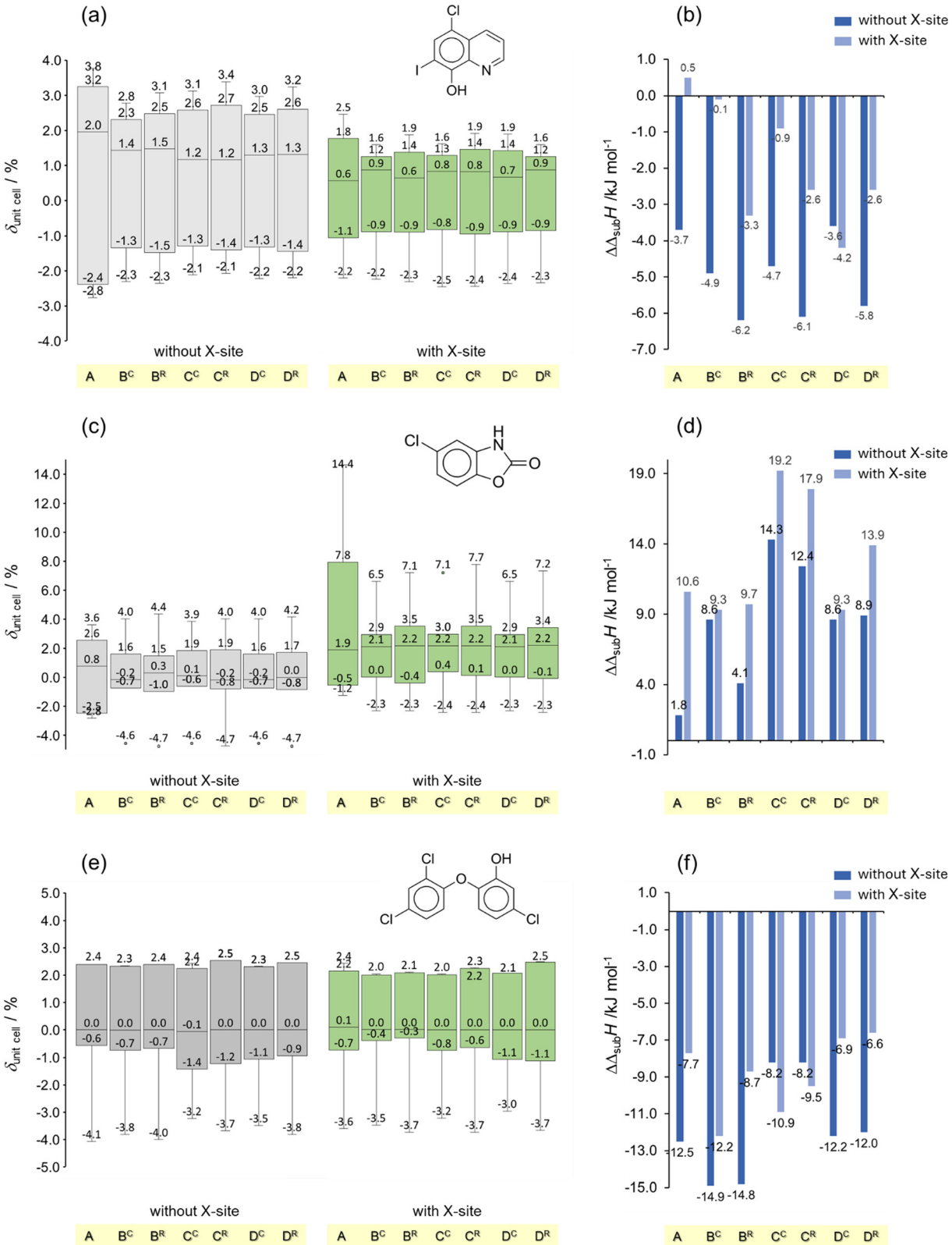

Fig. 3 Box plots obtained from the deviations between the computed (with and without an X-site in the model) and experimental unit cell parameters ($\delta_{unit\ cell}$) and enthalpies of sublimation ($\Delta\Delta_{sub}H$) for (a) and (b) clioquinol, CL; (c) and (d) chlorzoxazone, CZ; and (e) and (f) triclosan, TR. In panels (a), (c) and (e) the boxes represent the interquartile range (IQR), with the central line indicating the median of the values. The upper and lower edges correspond to the 75th and 25th percentiles, respectively. The whiskers extend to the smallest and largest values within 1.5 times the IQR from the quartiles.

parametrization in OPLS-AA needs to be reassessed to account for this type of molecular structure. Such task is, however, outside the scope of this work, since it will require a reparameterization of the model using a large set of experimental data for zwitterionic molecules.

The results obtained for the halogenated compounds (cliquinol, chlorzoxazone, and triclosan) with and without considering X-sites are compared in Fig. 3. Fig. 3 shows that, when only chlorine is present in the molecule (CZ and TR) no significant accuracy gain in the prediction of volumetric and energetic properties is obtained by considering the Cl σ-hole (Fig. 3c–f). In contrast, modelling the I σ-hole of CL, led to better agreement between the calculated and benchmark values of unit cell dimensions and enthalpy of sublimation (Fig. 3a and b). This probably reflects the ability of iodine to form stronger halogen bonds than chlorine.[80]

4 Conclusions

In summary, model D^C is the one that gave the best overall performance and is, therefore, recommended here to study organosulfur and organohalogen molecules of the types included in our test set. It is also advised that for halogenated molecules X-sites mimicking the σ-hole in these atoms are considered in the calculations, particularly if they contain iodine.

Also worth noting is the fact that all modified force fields considered here performed better than the original OPLS-AA model, both in terms of unit cell dimensions and enthalpy of sublimation predictions.

Last but not the least, the observation that all models tested performed poorer in terms of lattice energy than volumetric properties prediction, stresses again the importance of using both these types of data in the validation of new force fields.

Conflicts of interest

There are no conflicts to declare.

Data availability

The data supporting this article have been included as part of the ESI.†

Acknowledgements

This work was supported by FCT, Portugal, through projects UIDB/00100/2020 (**https://doi.org/10.54499/UIDP/00100/2020**), UIDP/00100/2020 (**https://doi.org/10.54499/UIDB/00100/2020**), LA/P/0056/2020 (**https://doi.org/10.54499/LA/P/0056/2020**), 2021.03239.CEECIND (**https://doi.org/10.54499/2021.03239.CEECIND/CP1650/CT0003**), 2023.12474.PEX (**https://doi.org/10.54499/2023.12474.PEX**), and the grant awarded to C. S. D. Lopes (SFRH/BD/128794/2017, COVID/BD/152581/2022). We also thank Prof. M. C. Oliveira (CQE-IST, Portugal) for the HPLC-ESI/MS analysis and Dr Ana Mourato for the PXRD analysis. Finally, we thank COST Action CA22107 – Bringing Experiment and Simulation Together in Crystal Structure Prediction (BEST-CSP), for providing a forum where helpful discussions related to the present work were promoted.

References

1 C. Chipot, *J. Phys. Chem. B*, 2024, **128**, 12023–12026.
2 T. Yagasaki, M. Matsumoto and H. Tanaka, *J. Chem. Theory Comput.*, 2020, **16**, 2460–2473.
3 D. Gobbo, P. Ballone, S. Decherchi and A. Cavalli, *J. Chem. Theory Comput.*, 2020, **16**, 4126–4140.
4 R. G. Simões, P. L. T. Melo, C. E. S. Bernardes, M. T. Heilmann, F. Emmerling and M. E. Minas da Piedade, *Cryst. Growth Des.*, 2021, **21**, 544–551.
5 A. Gavezzotti, *Chem. – Eur. J.*, 1999, **5**, 567–576.
6 H. Y. Tian, H. J. Zhang, J. L. Zhang and Y. Han, *J. Phys. Chem. C*, 2023, **127**, 1507–1518.
7 D. Golodnizky, C. E. S. Bernardes and M. Davidovich-Pinhas, *Food Chem.*, 2023, **439**, 138066.
8 R. G. Simões, C. E. S. Bernardes, A. Joseph, M. F. M. Piedade, W. Kraus, F. Emmerling, H. P. Diogo and M. E. Minas da Piedade, *Mol. Pharmaceutics*, 2018, **15**, 5349–5360.
9 R. G. Simões, C. S. D. Lopes, M. F. M. Piedade, C. E. S. Bernardes, H. P. Diogo and M. E. Minas da Piedade, *Cryst. Growth Des.*, 2020, **20**, 2321–2336.
10 F. Jensen, *Introduction to Computational Chemistry*, John Wiley & Sons, Chichester, UK, Hoboken, NJ, 3rd edn, 2017.
11 W. L. Jorgensen, D. S. Maxwell and J. Tirado-Rives, *J. Am. Chem. Soc.*, 1996, **118**, 11225–11236.
12 W. D. Cornell, P. Cieplak, C. I. Bayly, I. R. Gould, K. M. Merz, D. M. Ferguson, D. C. Spellmeyer, T. Fox, J. W. Caldwell and P. A. Kollman, *J. Am. Chem. Soc.*, 1996, **118**, 2309.
13 D. E. Williams, *J. Mol. Struct.*, 1999, **485**, 321–347.
14 C. E. S. Bernardes, M. E. Minas da Piedade and J. N. Canongia Lopes, *J. Phys. Chem. B*, 2012, **116**, 5179–5184.
15 J. Nyman, O. S. Pundyke and G. M. Day, *Phys. Chem. Chem. Phys.*, 2016, **18**, 15828–15837.
16 C. M. Breneman and K. B. Wiberg, *J. Comput. Chem.*, 1990, **11**, 361–373.
17 W. D. Cornell, P. Cieplak, C. I. Bayly and P. A. Kollman, *J. Am. Chem. Soc.*, 1993, **115**, 9620–9631.
18 A. Gavezzotti, *Z. Kristallogr.*, 2005, **220**, 499–510.
19 M. Leslie, *Mol. Phys.*, 2008, **106**, 1567–1578.
20 C. E. S. Bernardes and A. Joseph, *J. Phys. Chem. A*, 2015, **119**, 3023–3034.
21 C. E. S. Bernardes, M. T. Donato, M. F. M. Piedade, H. P. Diogo, J. N. Canongia Lopes and M. E. Minas da Piedade, *J. Chem. Thermodyn.*, 2019, **133**, 60–69.
22 A. O. L. Évora, D. F. Valente-Matias, C. E. S. Bernardes, C. M. Lousada, M. F. M. Piedade, M. Lusi, H. P. Diogo and M. E. Minas da Piedade, *Cryst. Growth Des.*, 2024, **24**, 9465–9481.

23 C. R. Groom, I. J. Bruno, M. P. Lightfoot and S. C. Ward, *Acta Crystallogr.*, 2016, **B72**, 171–179.
24 W. Acree and J. S. Chickos, *J. Phys. Chem. Ref. Data*, 2016, **45**, 033101.
25 W. Acree and J. S. Chickos, *J. Phys. Chem. Ref. Data*, 2017, **46**, 013104.
26 W. Acree and J. S. Chickos, *J. Phys. Chem. Ref. Data*, 2022, **51**, 043101.
27 J. S. Chickos and A. Gavezzotti, *Cryst. Growth Des.*, 2019, **19**, 6566–6576.
28 J. Laugier and B. Bochu, *CELREF V3: LMGP-Suite Suite of Programs for the interpretation of X-ray Experiments*, ENSP/Laboratoire des Matériaux et du Génie Physique, 1997, **https://www.ccp14.ac.uk/tutorial/lmgp/**.
29 G. M. Sheldrick, *SHELXL-97: Program for the Refinement of Crystal Structure*, University of Göttingen, Germany, 1997.
30 C. E. S. Bernardes, I. O. Feliciano, C. Naese, F. Emmerling and M. E. Minas da Piedade, *J. Chem. Thermodyn.*, 2023, **186**, 107137.
31 A. M. O'Connell and E. N. Maslen, *Acta Crystallogr.*, 1967, **22**, 134–145.
32 I. Ciocazanu and V. Meltzer, *J. Therm. Anal.*, 1996, **47**, 1755–1758.
33 S. Toscani, S. Thorén, V. Agafonov, R. Céolin and J. Dugué, *Pharm. Res.*, 1995, **12**, 1453–1456.
34 F. Martínez and A. Gómez, *J. Solution Chem.*, 2001, **30**, 909–923.
35 M. Przybyłek, P. Walczak, D. Ziółkowska, I. Grela and P. Cysewski, *J. Chem. Thermodyn.*, 2021, **153**, 106308.
36 Z. J. Cárdenas, D. M. Jiménez, O. A. Almanza, A. Jouyban, F. Martínez and W. E. Acree, *J. Solution Chem.*, 2016, **45**, 1479–1503.
37 A. K. Basak, S. Chaudhuri and S. K. Mazumdar, *Acta Crystallogr.*, 1984, **C40**, 1848–1851.
38 R. N. Nagrimanov, A. R. Italmasov, A. V. Buzyurov, S. E. Lapuk, R. A. Larionov, A. V. Gerasimov and M. A. Ziganshin, *J. Therm. Anal. Calorim.*, 2024, **149**, 1433–1442.
39 D. R. Mantheni, M. P. K. Maheswaram, R. Munigeti, I. Perera, A. Riga and K. S. Alexander, *J. Therm. Anal. Calorim.*, 2014, **115**, 2253–2260.
40 Y. Miyako, N. Khalef, K. Matsuzaki and R. Pinal, *Int. J. Pharm.*, 2010, **393**, 48–54.
41 S. Íde and A. Topaçh, *J. Chem. Crystallogr.*, 1997, **27**, 303–306.
42 J. A. Baird, B. V. Eerdenbrugh and L. S. Taylor, *J. Pharm. Sci.*, 2010, **99**, 3787–3806.
43 X. He, Y. J. Jiang, H. P. Zhou and Q. H. Zhu, *ChemistrySelect*, 2021, **6**, 5191–5194.
44 G. Padmanabhan, I. Becue and J. B. Smith, *Anal. Profiles Drug Subst.*, 1990, **18**, 57–90.
45 J. N. Latosińska, M. Latosińska, M. A. Tomczak, J. Seliger, V. Žagar and J. K. Maurin, *Magn. Reson. Chem.*, 2012, **50**, 89–105.
46 J. Lim, S. Jang, M. S. Shin and H. Kim, *Fluid Phase Equilib.*, 2012, **332**, 144–150.
47 T. Kiyobayashi and M. E. Minas da Piedade, *J. Chem. Thermodyn.*, 2001, **33**, 11–21.
48 C. E. S. Bernardes, L. M. N. B. F. Santos and M. E. Minas da Piedade, *Meas. Sci. Technol.*, 2006, **17**, 1405–1408.
49 *Computational Thermochemistry. Prediction and Estimation of Molecular Thermodynamics*, ed. K. K. Irikura and D. J. Frurip, ACS Symposium Series No. 677, Washington, 1998.
50 C. Lee, W. Yang and R. G. Parr, *Phys. Rev. B: Condens. Matter Mater. Phys.*, 1988, **37**, 785–789.
51 R. A. Kendall, T. H. Dunning and R. J. Harrison, *J. Chem. Phys.*, 1992, **96**, 6796–6806.
52 A. D. Becke, *J. Chem. Phys.*, 1993, **98**, 5648–5652.
53 D. E. Woon and T. H. Dunning, *J. Chem. Phys.*, 1993, **98**, 1358–1371.
54 NIST Computational Chemistry Comparison and Benchmark Database, NIST Standard Reference Database Number 101, Release 22, May 2022, DOI: **10.18434/T47C7Z**, **https://cccbdb.nist.gov/**.
55 M. N. Glukhovtsev, A. Pross, M. P. Mcgrath and L. Radom, *J. Chem. Phys.*, 1995, **103**, 1878–1885.
56 B. P. Pritchard, D. Altarawy, B. Didier, T. D. Gibson and T. L. Windus, *J. Chem. Inf. Model.*, 2019, **59**, 4814–4820.
57 M. J. Frisch, G. W. Trucks, H. B. Schlegel, G. E. Scuseria, M. A. Robb, J. R. Cheeseman, G. Scalmani, V. Barone, B. Mennucci, G. A. Petersson, H. Nakatsuji, M. Caricato, X. Li, H. P. Hratchian, A. F. Izmaylov, J. Bloino, G. Zheng, J. L. Sonnenberg, M. Hada, M. Ehara, K. Toyota, R. Fukuda, J. Hasegawa, M. Ishida, T. Nakajima, Y. Honda, O. Kitao, H. Nakai, T. Vreven, J. A. Montgomery Jr., J. E. Peralta, F. Ogliaro, M. J. Bearpark, J. Heyd, E. N. Brothers, K. N. Kudin, V. N. Staroverov, R. Kobayashi, J. Normand, K. Raghavachari, A. P. Rendell, J. C. Burant, S. S. Iyengar, J. Tomasi, M. Cossi, N. Rega, N. J. Millam, M. Klene, J. E. Knox, J. B. Cross, V. Bakken, C. Adamo, J. Jaramillo, R. Gomperts, R. E. Stratmann, O. Yazyev, A. J. Austin, R. Cammi, C. Pomelli, J. W. Ochterski, R. L. Martin, K. Morokuma, V. G. Zakrzewski, G. A. Voth, P. Salvador, J. J. Dannenberg, S. Dapprich, A. D. Daniels, Ö. Farkas, J. B. Foresman, J. V. Ortiz, J. Cioslowski and D. J. Fox, *Gaussian 09, Revision D.01*, Gaussian, Inc., New York, 2009.
58 C. I. Bayly, P. Cieplak, W. D. Cornell and P. A. Kollman, *J. Phys. Chem.*, 1993, **97**, 10269–10280.
59 T. Lu and F. W. Chen, *J. Comput. Chem.*, 2012, **33**, 580–592.
60 F. Neese, *Wiley Interdiscip. Rev.: Comput. Mol. Sci.*, 2022, **12**, e1606.
61 P. J. Stephens, F. J. Devlin, C. F. Chabalowski and M. J. Frisch, *J. Phys. Chem.*, 1994, **98**, 11623–11627.
62 S. Grimme, J. Antony, S. Ehrlich and H. Krieg, *J. Chem. Phys.*, 2010, **132**, 154104.
63 F. Weigend and R. Ahlrichs, *Phys. Chem. Chem. Phys.*, 2005, **7**, 3297–3305.
64 F. Weigend, *Phys. Chem. Chem. Phys.*, 2006, **8**, 1057–1065.
65 F. Neese, F. Wennmohs, A. Hansen and U. Becker, *Chem. Phys.*, 2009, **356**, 98–109.
66 J. G. Brandenburg, C. Bannwarth, A. Hansen and S. Grimme, *J. Chem. Phys.*, 2018, **148**, 064104.
67 M. J. Frisch, M. Head-Gordon and J. A. Pople, *Chem. Phys. Lett.*, 1990, **166**, 275–280.

68 M. J. Frisch, M. Head-Gordon and J. A. Pople, *Chem. Phys. Lett.*, 1990, **166**, 281–289.
69 A. P. Thompson, H. M. Aktulga, R. Berger, D. S. Bolintineanu, W. M. Brown, P. S. Crozier, P. J. I. Veld, A. Kohlmeyer, S. G. Moore, T. D. Nguyen, R. Shan, M. J. Stevens, J. Tranchida, C. Trott and S. J. Plimpton, *Comput. Phys. Commun.*, 2022, **271**, 10817.
70 C. E. S. Bernardes, *J. Chem. Inf. Model.*, 2022, **62**, 1471–1478.
71 R. W. Hockney and J. W. Eastwood, *Computer Simulation Using Particles*, A. Hilger, Bristol England, Philadelphia, 1988.
72 E. Tiesinga, P. J. Mohr, D. B. Newell and B. N. Taylor, *Rev. Mod. Phys.*, 2021, **93**, 033105.
73 J. N. Canongia Lopes, P. Cabral do Couto and M. E. Minas da Piedade, *J. Phys. Chem. A*, 2006, **110**, 13850–13856.
74 C. E. S. Bernardes and J. N. Canongia Lopes, *J. Chem. Theory Comput.*, 2017, **13**, 6167–6176.
75 M. Schauperl, P. S. Nerenberg, H. Jang, L. P. Wang, C. I. Bayly, D. L. Mobley and M. K. Gilson, *Commun. Chem.*, 2020, **3**, 44.
76 W. L. Jorgensen and P. Schyman, *J. Chem. Theory Comput.*, 2012, **8**, 3895–3901.
77 I. T. Todorov, W. Smith, K. Trachenko and M. T. Dove, *J. Mater. Chem.*, 2006, **16**, 1911–1918.
78 M. A. V. Ribeiro da Silva and M. J. S. Monte, *J. Chem. Thermodyn.*, 1992, **24**, 715–724.
79 J. A. Pople, *Rev. Mod. Phys.*, 1999, **71**, 1267–1274.
80 G. Cavallo, P. Metrangolo, R. Milani, T. Pilati, A. Priimagi, G. Resnati and G. Terraneo, *Chem. Rev.*, 2016, **116**, 2478–2601.